Pergamon

Geochimica et Cosmochimica Acta, Vol. 66, No. 16, pp. 2875–2885, 2002

0016-7037/02 $22.00 + .00

PII S0016-7037(02)00888-8

EXAFS study of rare-earth element coordination in calcite

E. J. Elzinga,[1] R. J. Reeder,[1,*] S. H. Withers,[2] R. E. Peale,[2] R. A. Mason,[3] K. M. Beck[4] and W. P. Hess[4]

[1]Department of Geosciences, State University of New York at Stony Brook, Stony Brook, NY 11794-2100, USA
[2]Department of Physics, University of Central Florida, Orlando, FL 32816-2385, USA
[3]Department of Earth Sciences, Memorial University of Newfoundland, St. John's, Newfoundland, Canada, A1B 3X5
[4]Environmental Molecular Sciences Laboratory, Pacific Northwest National Laboratory, Richland, WA 99352, USA

(*Received September* 4, 2001; *accepted in revised form March* 11, 2002)

Abstract—Extended X-ray absorption fine-structure (EXAFS) spectroscopy is used to characterize the local coordination of selected rare-earth elements (Nd^{3+}, Sm^{3+}, Dy^{3+}, Yb^{3+}) coprecipitated with calcite in minor concentrations from room-temperature aqueous solutions. Fitting results confirm substitution in the Ca site, but first-shell Nd-O and Sm-O distances are longer than the Ca-O distance in calcite and longer than what is consistent with ionic radii sums for sixfold coordination in the octahedral Ca site. In contrast, first-shell Dy-O and Yb-O distances are shorter than the Ca-O distance and are consistent with ionic radii sums for sixfold coordination. Comparison of Nd-O and Sm-O bond lengths with those in lanthanide sesquioxides and with ionic radii trends across the lanthanide series suggests that Nd^{3+} and Sm^{3+} have sevenfold coordination in a modified Ca site in calcite. This would require some disruption of the local structure, with an expected decrease in stability, and possibly a different charge compensation mechanism between Nd and Sm vs. Yb and Dy. A possible explanation for the increased coordination for the larger rare-earth elements involves bidentate ligation from a CO_3 group. Because trivalent actinides such as Am^{3+} and Cm^{3+} have ionic radii similar to Nd^{3+}, their incorporation in calcite may result in a similar defect structure.

1. INTRODUCTION

Rare-earth element (REE) patterns have long been recognized as valuable indicators of provenance and alteration for minerals and rocks. Ca-bearing minerals are commonly enriched in REEs relative to other phases, reflecting the ease with which REEs substitute for Ca. The REEs usually occur as trivalent ions and show similar chemical behaviors owing to their electronic configurations. Ce and Eu also occur in other oxidation states, which is sometimes reflected in their enrichment patterns. A notable difference among the trivalent ions is a decrease in ionic radius with increasing atomic number, which is known as the lanthanide contraction. The size range covered by the trivalent REEs encompasses that of Ca, and this similarity is one reason for the compatibility of trivalent REEs with Ca-bearing phases, despite the difference in charge. Relatively few studies have addressed the incorporation of REEs into calcium carbonate, despite the widespread occurrence of calcite and aragonite in sediments and sedimentary rocks. More recently, interest in trivalent REEs in carbonate systems has developed because of expected similarities with the chemical behavior of trivalent actinide species (e.g., Am^{3+}, Cu^{3+}, Pu^{3+}), which pose serious threats as contaminants associated with radionuclide waste sources. The use of REEs as analogs avoids some of the difficulties associated with handling actinides in experiments. Uptake by calcite and other carbonates may influence the mobility and fate of actinides in the near-surface environment.

Both experimental studies (Terakado and Masuda, 1988; Zhong and Mucci, 1995) and field studies (Parekh et al., 1977; Palmer, 1985) have shown that REEs are strongly partitioned into calcite during growth. Terakado and Masuda (1988) reported apparent partition coefficients for REE coprecipitation in batch experiments ranging from 2.5 to 10. Based on more carefully designed experiments, Zhong and Mucci (1995) reported partition coefficients from $\sim 10^{3.6}$ for La^{3+}, decreasing systematically with atomic number, to $\sim 10^{1.9}$ for Yb^{3+}. REE concentrations in calcitic marine sediments and marine biogenic calcite suggest that effective partition coefficients (in seawater) may be slightly lower than those given by Zhong and Mucci (1995). Nevertheless, it is clear that REEs should be effectively scavenged from solutions in which calcite is precipitating, even in small quantities.

A fundamental question for any heterovalent substitution is the charge compensation mechanism. Zhong and Mucci (1995) observed that Na^+ coprecipitation (from seawater-like solutions) was linearly correlated with REE coprecipitation. On this basis, they argued that REEs substitute in the Ca site and that coprecipitation of Na^+ may compensate for the trivalent charge of the REE. Presumably that would be effective only if Na^+ or another monovalent ion were a near neighbor of the REE^{3+} and substituting for a Ca^{2+}. However, it is also possible that local coordination of the REE is affected in other ways.

Other potentially important aspects for REE coprecipitation with calcite are aqueous speciation and adsorption. In solutions that are saturated or supersaturated with calcite, the dominant aqueous REE species are predicted to be the carbonate complexes $REECO_3^+$ and/or $REE(CO_3)_2^-$, depending on pH (Wood, 1990; Millero, 1992; Lee and Byrne, 1993). Zhong and Mucci (1995) reported results from kinetic batch experiments of trivalent REE adsorption to calcite in saturated solutions. They found a strong affinity of REEs for the calcite surface, with an initial rapid uptake followed by slower uptake. No

* Author to whom correspondence should be addressed (rjreeder@notes.cc.sunysb.edu).

evidence of a separate REE precipitate was observed. In contrast, Carroll et al. (1992) and Carroll (1993) examined the interaction of Nd^{3+} with calcite in saturated solutions and observed precipitation of a discrete Nd carbonate or Nd-Ca carbonate phase at the surface. Differences in solution chemistry or experimental procedures may account for the different results, but both sets of studies suggest that other rapid reactions, in addition to coprecipitation, may contribute to uptake of REEs at the calcite-water surface. Moreover, several workers have emphasized that a continuum may exist between adsorption and (co-)precipitation as processes responsible for metal uptake by carbonates (Davis et al., 1987; Xu et al., 1996). Hence, for time scales relevant to contamination history and to many geologic processes, the formation of dilute solid solutions may represent the final state of metals in carbonate systems.

Our focus in the present study is to characterize the structural environment of REEs in dilute calcite solid solutions. We used extended X-ray absorption fine structure (EXAFS) spectroscopy to examine the local coordination of selected REE^{3+} samples coprecipitated with calcite. We considered Nd, Sm, Dy, and Yb, choices partly constrained by practical considerations but nevertheless spanning a significant portion of the lanthanide series. Because concentrations of REEs in natural calcite are generally too low for EXAFS study, we have synthesized a series of calcites with relatively high REE concentrations. Our results confirm that REEs occupy the Ca site as expected, but also indicate that the light REEs (LREEs) Nd and Sm adopt a different local coordination than heavy REEs (HREEs) Dy and Yb. This difference should be reflected in the stabilities of the dilute solid solutions and may therefore lead to differences between LREEs and HREEs with respect to long-term retention by calcite.

2. MATERIAL AND METHODS

2.1. Coprecipitation Procedures

The Nd-, Sm-, and Dy-doped calcite samples were synthesized at room temperature in aqueous solutions using a modified free-drift method based on that described by Gruzensky (1967): Growth occurs in a sealed reaction vessel with headspace in contact with a reservoir of solid ammonium carbonate. Near-steady-state decomposition of the ammonium carbonate produces NH_3(g) and CO_2(g), which dissolve into a solution containing $CaCl_2$, simultaneously increasing pH and carbonate alkalinity until calcite crystallization occurs. The use of a background electrolyte (NH_4Cl) at high ionic strength (3–5 molal) facilitates steady-state growth of crystals over a period of 1 to 2 weeks with relatively constant pH (7.5–7.7) (Paquette and Reeder, 1995). This technique produces single crystals up to 600 μm and larger aggregates of crystals. The linear growth rates obtained with this technique were in the range of 1 to 5 $\times$ 10^{-8} cm s^{-1}. The disadvantage of this approach is that, despite the nearly constant pH during the coprecipitation period, the initial Ca and REE concentrations decrease over the duration of the experiment and, hence, the solution composition does not remain constant. This should not pose a problem for the current work, assuming that the mode of incorporation remains the same as the solution composition changes.

The Sm- and Dy-doped calcite crystals are from the study of Mason and Mariano (1990), who give further details of preparation. Their luminescence images show that these calcite samples exhibit growth zoning of the individual REE, presumably reflecting the changes in solution composition during crystal growth. Although the Nd-doped calcite was grown by the same method as the Sm and Dy samples, i.e., the modified Gruzensky (1967) method, X-ray microprobe mapping indicated a more uniform Nd concentration throughout. The crystals and aggregates at least partly exhibit the common growth form $\{10\bar{1}4\}$ but with irregular morphologies, as well as some different forms. In contrast, calcite grown in the presence of divalent metals nearly always exhibits well-developed $\{10\bar{1}4\}$ faces (Reeder, 1996).

The Yb-doped calcite was synthesized at room temperature using a constant-addition method described by Reeder et al., (2001). $CaCl_2$ and $NaHCO_3$ solutions were delivered at a constant rate using a dual-syringe pump to a stirred reaction vessel through which air was bubbled continuously. Solution Ca and HCO_3 concentrations were maintained at ~5 mM. NaCl was used as a background electrolyte to give an ionic strength of 0.1 molal. The pH initially increased until calcite nucleation was observed, then dropped to 8.1 to 8.3 and remained relatively constant throughout the duration of the coprecipitation experiment. Aqueous Yb^{3+} solution was added after the pH stabilized to give an initial solution concentration of 15 μM. The $CaCl_2$ syringe also contained a predetermined amount of Yb^{3+} to account for that taken up by calcite during growth. Solutions were undersaturated with respect to $Yb_2(CO_3)_3{\cdot}xH_2O$. The average growth rate of this sample during the 45-h synthesis period employed was 1.5×10^{-4} mol m^{-2} h^{-1}. The finely crystalline calcite product was recovered by vacuum filtration, washed in deionized water, and dried at 50°C.

X-ray diffraction failed to reveal any reflections other than those for calcite, and no differences between pure calcite and the REE-doped calcites were found, which reflects the dilute nature of the REE-calcite solid solutions. Approximate REE concentrations in the calcites were determined by Rutherford backscattering, ICP-MS, or spatially resolved X-ray fluorescence and are as follows: Nd, 3594 ppm; Sm, 1748 ppm; Dy, 1869 ppm; and Yb, 885 ppm. Samples were ground to a fine powder for bulk EXAFS analyses.

2.2. EXAFS Spectroscopy

EXAFS spectra of the Sm-, Dy-, and Yb-doped calcites were collected at beamline X11A of the National Synchrotron Light Source (NSLS) at Brookhaven National Laboratory. The NSLS storage ring was operated at 2.5 or 2.8 GeV with a maximum current of 290 mA. Scans were taken over the L_3-edges using a pair of Si(111) monochromator crystals, with one crystal detuned by ~35 to 40% for harmonic rejection. Samples were mounted in cavities in aluminum holders covered with Kapton tape and secured in a cold-finger positioned at 45° to the X-ray beam. Samples were held near 77 K using a liquid nitrogen cryostat, which improved the signal/noise ratio. The fluorescence yield was monitored using a 13-element solid-state Ge detector. Spectra of Sm_2O_3, Dy_2O_3, and Yb_2O_3 were collected using transmission methods for use as model compounds. Reference spectra were also collected for $Nd_2(CO_3)_3{\cdot}xH_2O$,

$Sm_2(CO_3)_3{\cdot}xH_2O$, $Dy_2(CO_3)_3{\cdot}xH_2O$, and $Yb_2(CO_3)_3{\cdot}xH_2O$. Spectra for the Nd, Sm, Dy, and Yb samples were calibrated by assigning the first inflection point to the tabulated threshold energy values 6208, 6716, 7790, and 8944 eV, respectively.

Spectra for the Nd-doped calcite were collected at beamline 20-ID-B of the Advanced Photon Source (APS) at Argonne National Laboratory. The APS storage ring was operated at 7 GeV with a maximum current of 100 mA. Nd-doped calcite samples were ground into fine powder and spread evenly onto clear tape. Nine layers of this calcite-coated tape were placed in the beam to produce the desired edge step. Si(111) monochromator crystals were used to produce a monochromatic beam, with one crystal detuned 25% for reduction of harmonics. The Nd L_3-edge fluorescence yield was measured with a 13-element Ge detector. The sample was cooled near 77 K using a liquid nitrogen cryostat.

Data analysis included subtraction of a linear preedge background, normalization, and conversion to k-space, followed by μ_0 fitting using a cubic spline. The $\chi(k)$ function was Fourier transformed using k^3 weighting, and all fitting was done in R-space using the program WinXAS2.0 (Ressler, 1997) and theoretical backscattering amplitudes and phase shifts were calculated using FEFF7 (Zabinsky et al., 1995). Starting models used for the FEFF7 calculations were based on the REE dopant placed at the Ca position in calcite. A single threshold energy value (ΔE_0) was allowed to vary during fitting. Typical k and R ranges were 2 to 11 $Å^{-1}$ and 0.3 to 4.1 Å, respectively, and the number of parameters allowed to vary during fitting was always less than the Nyquist limit. The amplitude reduction factor, S_0^2, was fixed at a value of one. This value was determined from fitting the REE_2O_3 reference compounds, which yielded values in the range 0.96 to 1.0. These reference compounds contain, however, multiple REE sites with split first O shells, thereby complicating a truly accurate determination of S_0^2 for each individual REE, which is why we chose to fix this value at 1.0 in all cases. Errors in the fit parameters, estimated from fits of well-characterized model compounds, are ± 20% for coordination number (N), ± 0.02 Å for first and second shell distances (R), and ± 0.03 Å for greater distances. Debye-Waller-type factors (σ^2) have an approximate error of ± 0.002 $Å^2$.

3. RESULTS

The near-edge regions of the normalized L_3-edge absorption spectra are shown in Figure 1 The REE-doped calcite spectra are generally similar in appearance, all showing a characteristic intense white line feature. The REE-doped calcite spectra differ in detail from the spectra of the corresponding REE-carbonates and -oxides (Fig. 1), which is more evident in the k^3-weighted EXAFS (Fig. 2). The small preedge feature appearing as a shoulder on the Sm-doped calcite spectrum is not present in the Sm_2O_3 and $Sm_2(CO_3)_3{\cdot}xH_2O$ reference spectra, and may therefore indicate the presence of a small amount of divalent Sm in this sample, possibly due to the growth medium, which had a high concentration of background NH_4Cl used for synthesizing the sample.

There is no evidence of features in any of the EXAFS spectra attributable to multi-electron excitations such as those described by Solera et al., (1995) and D'Angelo et al., (2001) for aqueous REE(III) compounds. Fourier transform (FT) magnitudes (Fig. 3) of all calcite:REE^{3+} spectra are dominated by a single low-R peak at ~1.8 Å (uncorrected for phase shift) attributable to the first shell of oxygen atoms. Smaller peaks at higher R are consistent with shells from C, O, and Ca and indicate occupation of the REE^{3+} at the unique Ca site, as discussed below. Best-fit parameters are given in Table 1 and selected fits in R-space are shown in Figure 4.

The observed first-shell REE-O distances decrease systematically across the series, being 2.41, 2.38, 2.30, and 2.24 Å for Nd, Sm, Dy, and Yb, respectively (Table 1). This trend is consistent with the decrease in REE^{3+} ionic radii from the light to the heavy ends of the series known as the lanthanide contraction. Fitted coordination numbers range from 7.5 to 9.5, which are larger than would be expected for occupation of the octahedral Ca site. However, the ± 20% error on these values makes it difficult to determine coordination number directly from EXAFS data fitting. Moreover, the N values are highly correlated with both the Debye-Waller-type values (σ^2) and the amplitude reduction factor (S_0^2), so the fitted distances (which are more accurate than the fitted coordination numbers) and fits of other shells must be used to confirm the REE site. As we note below, the first-shell REE-O distances, on closer inspection, suggest differences in coordination among these lanthanide ions in calcite.

For the Ca site of the ideal calcite structure, the shells beyond the first oxygen coordination include carbon (at 3.21 Å), a second oxygen shell (at 3.46 Å), and calcium (at 4.05 Å), each having ideal N values of 6 (Fig. 5). The Ca shell corresponds to the centers of the octahedra that share corners with the central absorber octahedron. A more distant Ca shell exists at 4.99 Å but was not considered in our fitting procedure. On the assumption that the local structure is largely like that in ideal calcite, except for localized expansion or contraction, coordination numbers for the carbon, second oxygen, and calcium shells were fixed at 6; this reduced the number of fit parameters needed. The fit quality obtained by using these four shells was visually good, but some discrepancies were evident beyond the Ca shell, indicating contributions from shells located beyond the Ca shell (Fig. 4). Best-fit REE-X distances (Table 1) for the carbon, second oxygen, and calcium shells also show a decrease from Nd to Yb, as would be expected for decreasing ionic radii. The REE-Ca distance varies systematically from 4.13 to 4.04 Å for Nd through Yb (Table 1). These distances are very near or just slightly greater than the Ca-Ca distance in ideal calcite (4.05 Å). This confirms that the REEs occupy the Ca position and is consistent with previous observations for divalent metal substitution showing that the M^{2+}-Ca distance deviates only slightly from the ideal value. As an exercise, we also attempted to fit this shell using the REE as the backscatterer. Although the fits obtained were reasonable, the similarity of the distance to that observed in calcite (and the dissimilarity to known REE-REE distances) support our interpretation that the REE elements are incorporated in the calcite structure forming a dilute solid solution and do not form a separate secondary phase or localized REE-rich inclusions within the calcite bulk. By constraining the coordination number in the carbon, second oxygen, and calcium shells to 6, large Debye-Waller-type factors are obtained for some shells, especially for

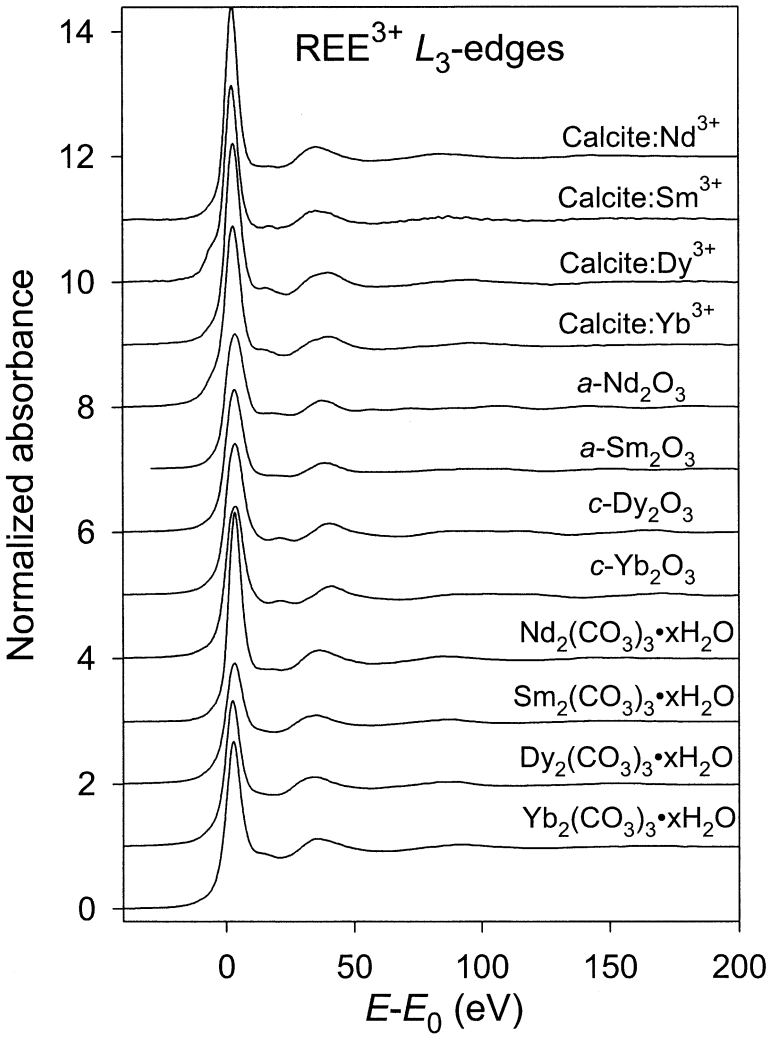

Fig. 1. The near-edge regions of the normalized REE L_3-edge absorption spectra of Nd-, Sm-, Dy-, and Yb-doped calcite. Also shown are the L_3-edge absorption spectra of solid REE_2O_3 and $REE_2(CO_3)_3 \cdot xH_2O$ reference standards (REE = Nd, Sm, Dy, and Yb).

the Ca shell. This may reflect real variations in this nearest metal site.

One limitation observed during the fitting was that the optimized parameters for the carbon and second oxygen shells were strongly correlated due to the overlap between these shells, which were typically separated by 0.2 to 0.3 Å. The fitting results for these shells are, therefore, less accurate than for the REE-O and REE-Ca shells. No evidence of a significant contribution from multiple scattering was found, although Reeder et al., (1999) noted a weak contribution in Co^{2+}- and Zn^{2+}-doped calcite.

4. DISCUSSION

The EXAFS fit results, accounting for oxygen, carbon, a second oxygen, and calcium shells, clearly support the occupation of the Nd^{3+}, Sm^{3+}, Dy^{3+}, and Yb^{3+} dopants at the Ca site in calcite, as was expected. The relatively small deviations of the observed REE-Ca distances from those in the ideal calcite structure also suggest that a significant amount of the structural relaxation associated with the heterovalent substitution is contained within the nearest several coordination shells, which is consistent with previous findings for divalent metal substitution in calcite (Reeder et al., 1999). Closer inspection of the first-shell oxygen distances, however, reveals some unexpected trends. The Nd-O distance in calcite:Nd (2.41 Å) is 0.05 Å greater than the Ca-O distance in ideal calcite (2.36 Å), yet the sixfold ionic radii of Nd^{3+} and Ca^{2+} are nearly identical at 0.983 and 1.00 Å, respectively (Shannon, 1976). This difference of 0.05 Å is greater than the associated estimated errors. The Sm-O distance in calcite:Sm (2.38 Å) is also slightly larger than the 2.36-Å Ca-O distance in calcite, yet the sixfold ionic radius of Sm^{3+} (0.958 Å) is smaller than that of Ca^{2+} (1.00 Å). In contrast, the Dy-O and Yb-O distances in calcite:Dy and calcite:Yb (2.30 and 2.24 Å, respectively) are proportionately smaller than the 2.36 Å Ca-O distance, as would be expected from their smaller ionic radii (Dy^{3+} at 0.912 Å and Yb^{3+} at

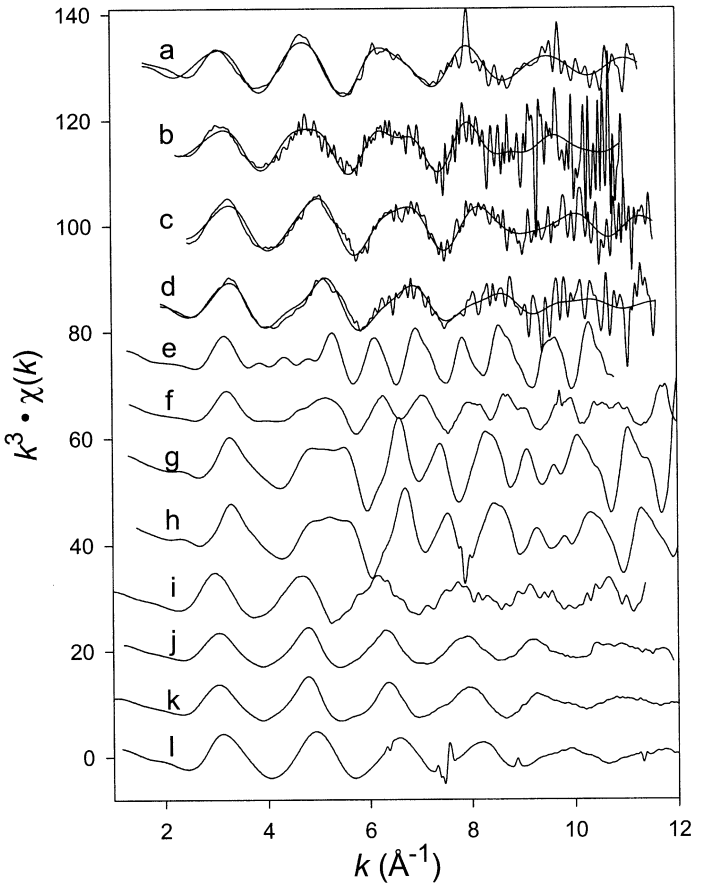

Fig. 2. The k^3-weighted $\chi(k)$ spectra for Nd, Sm, Dy, and Yb-doped calcites (a–d) compared with corresponding lanthanide sesquioxides (e–h) and the Nd, Sm, Dy, and Yb carbonate hydrates (i–l). Fits are shown for the calcite spectra.

0.868 Å; Shannon, 1976). Thus, the Nd-O and Sm-O distances appear anomalously large for the Ca site, whereas the Dy-O and Yb-O distances appear reasonable.

One of the principal findings of our previous EXAFS study of divalent metal substitution in calcite (Reeder et al., 1999) was the close similarity of the observed first-shell M^{2+}-O distances to corresponding distances found in pure endmember carbonates and to distances predicted from the sum of ionic radii (i.e., M + O). Cheng et al., (2001) and Lee et al., (2002) also found that the Mn-O distance in calcite:Mn^{2+} was nearly the same as in pure $MnCO_3$. This reflects that the first-shell bond distances are roughly conservative, a relationship noted elsewhere and not limited to the calcite structure (cf. Galoisy, 1996). Consequently, we would expect the first-shell distances of the REE dopants in calcite to be consistent with the appropriate ionic radii. Moreover, because slight differences in M-O distance exist among different structures even for a given coordination geometry, the observed trend for the REE-O distances should at least parallel the corresponding trends for the ionic radii.

A comparison of the observed REE^{3+}-O distances with values predicted from sixfold and from sevenfold ionic radii is shown in Fig. 6. Taken as a single trend, the observed REE-O distances do not seem to fit either trend line calculated from the sixfold and the sevenfold ionic radii from Shannon (1976). The observed Nd-O distance falls on the trend line for sevenfold coordination, with the Sm-O distance just slightly below it, and the Yb-O distance falls on the trend line for sixfold coordination, with the Dy-O distance slightly above it. This emphasizes the previous observation that the Nd-O and Sm-O distances in calcite are longer than would be expected for sixfold coordination. The Dy-O and Yb-O distances are, however, consistent with sixfold coordination. Because the EXAFS fits confirm that all four REEs occupy the Ca site, the most obvious interpretation is that differences in local coordination occur among the REE ions in calcite; the HREE impurities Dy and Yb are dominantly in sixfold coordination and the LREEs Nd and Sm are dominantly in sevenfold coordination, the latter being a modified Ca site.

The near-edge data shown in Figure 1 reveal a shoulder on the XANES spectrum of the Sm-calcite sample, perhaps indicating the presence of divalent Sm as noted previously. The possibility exists that Sm in this sample is present as a mixture of sixfold-coordinated Sm(III) and sevenfold or higher coordinated Sm(II). The Sm-O distance for sixfold Sm(III) is 2.33 Å (Shannon, 1976), and the Sm-O distance for sevenfold Sm(II) is 2.59 Å (Shannon, 1976). A mixture containing 80% sixfold Sm(III) and 20% sevenfold Sm(II) would give a weighted average $R_{Sm\text{-}O}$ of 2.38 Å, which is the first-shell $R_{Sm\text{-}O}$ found for the Sm-calcite sample (Table 1). Attempts to fit the O-shell

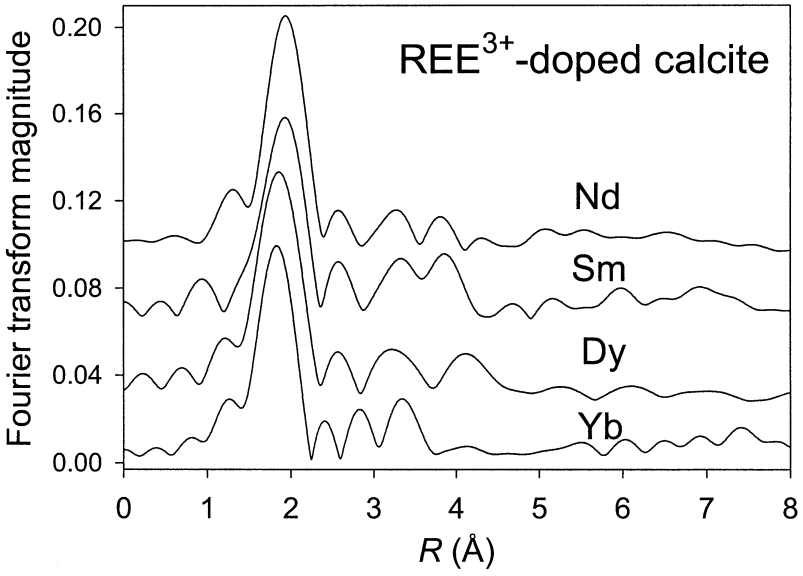

Fig. 3. Fourier transform (FT) magnitudes (not corrected for phase shifts) of the REE^{3+}-doped calcites.

of the Sm-doped calcite sample with a combination of O-shells located at 2.33 (±0.02) Å and 2.58 (±0.02) Å failed to give good results. Similar attempts for eightfold-coordinated Sm(II) ($R_{Sm\text{-}O}$ = 2.63 Å; Shannon, 1976) and ninefold Sm(II) ($R_{Sm\text{-}O}$ = 2.68 Å; Shannon, 1976) were also unsuccessful. This suggests that either the shoulder on the Sm-calcite spectrum is not the result of the presence of divalent Sm or that the contribution of divalent Sm, if present, was not significant.

A useful comparison of our observed REE-O distances in calcite is with those in another structure type in which the REE is known to be in sixfold coordination. Unfortunately, few studies have examined structural changes across the entire lanthanide series, and no data for REE carbonates are available for such a comparison. The most complete structural data exist for the *c*-sesquioxides (REE_2O_3), which have the bixbyite structure. There are two distinct REE sites in the *c* modification, both having sixfold coordination. The average REE-O distances in the different sites are similar (cf. Schleid and Meyer, 1989; Maslen et al., 1996), and the average REE-O distance from both can be used to document a trend for comparison with our values for calcite:REE. We were unable to find a reliable X-ray structure refinement for *c*-Nd_2O_3, perhaps reflecting that the *a*-modification is stable. However, well-defined trends for unit cell parameters and the single positional coordinate in the *c*-sesquioxide series allow confident prediction of the Nd-O distances (Hanic et al., 1984). Figure 7 shows that the average REE-O distance in the *c*-sesquioxides decreases linearly with increasing atomic number across the lanthanide series. Our observed Dy-O and Yb-O distances in calcite fall almost exactly on the trend formed by the REE-O distance in the *c*-sesquioxides. In contrast, our observed Nd-O and Sm-O distances lie distinctly above the trend and beyond estimated errors. This discrepancy for the LREEs Nd and Sm supports our inter-

Table 1. XAFS fit results for synthetic REE-doped calcite samples.

	REE-O_1			REE-C		
REE	*N*	*R* (Å)	σ^2 (Å^2)	*N**	*R* (Å)	σ^2 (Å^2)
Nd	9.5	2.41	0.008	6	3.26	0.018
Sm	8.3	2.38	0.009	6	3.24	0.008
Dy	7.9	2.30	0.007	6	3.21	0.006
Yb	7.5	2.24	0.008	6	3.14	0.010
	REE-O_2			REE-Ca		
	*N**	*R* (Å)	σ^2 (Å^2)	*N**	*R* (Å)	σ^2 (Å^2)
Nd	6	3.55	0.012	6	4.13	0.022
Sm	6	3.48	0.012	6	4.09	0.012
Dy	6	3.43	0.006	6	4.06	0.020
Yb	6	3.27	0.011	6	4.04	0.015

Estimated errors for coordination number (*N*) are ± 20%, for *R* ± 0.02 Å, and for σ^2 ± 0.002 Å^2.
* *N* fixed at value in ideal structure.

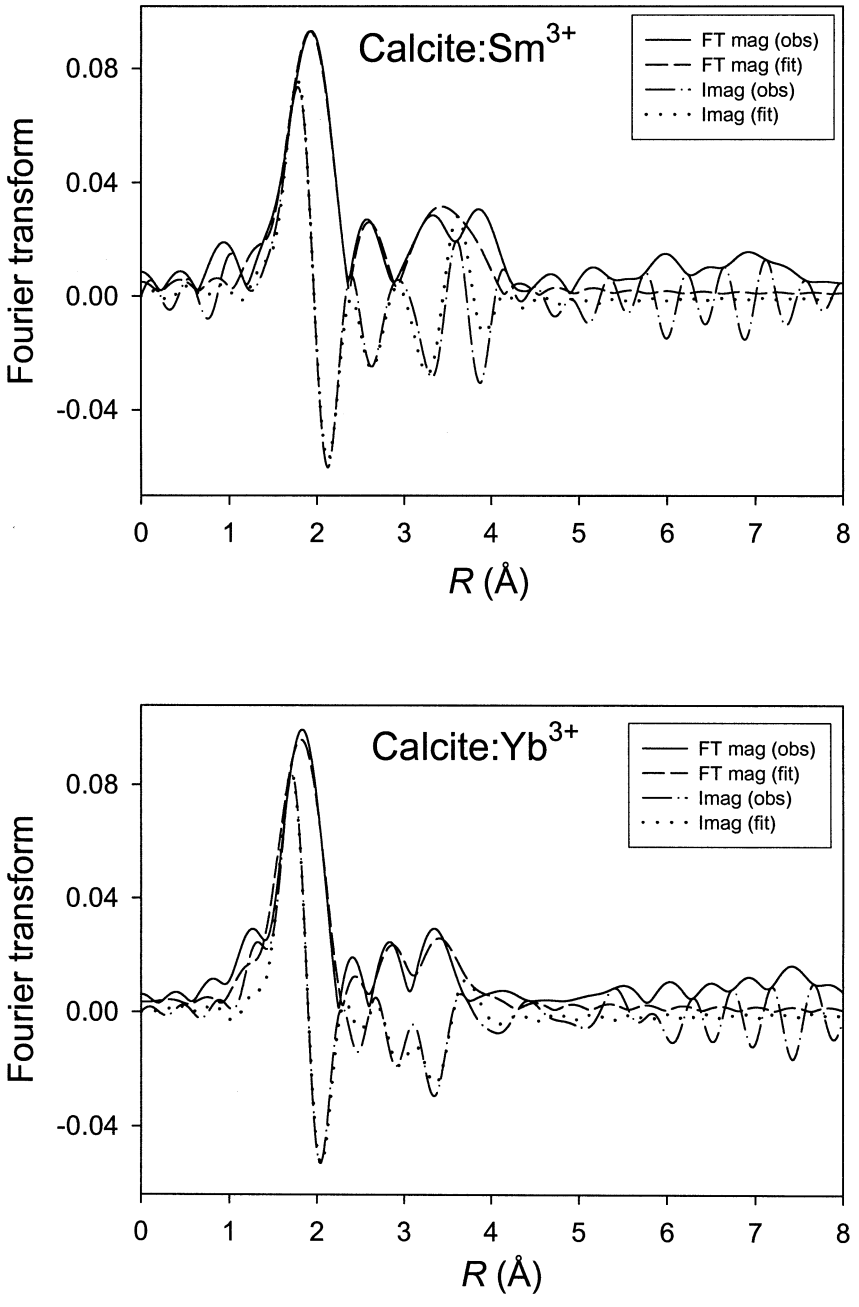

Fig. 4. Real and imaginary components of *R*-space fits for Sm- and Yb-doped calcites.

pretation that they have different coordination in calcite than the HREEs Dy and Yb.

The observation that the Nd-O and the Sm-O distances in calcite lie close to the trend line predicted for sevenfold coordination (Fig. 6) suggests this as the most likely interpretation of our EXAFS results, that seven oxygens form the first coordination shell of the larger REEs Nd and Sm. Initially, we questioned this result simply because of the disruption that would be required in the local structure. Moreover, our fits for more distant shells showed reasonable agreement with those expected for the ideal calcite structure.

Bond valence theory offers tentative support for our interpretation of different coordination among the REEs, although we note that there is inconsistency among the different bond valence parameters reported for certain trivalent lanthanide-oxygen bonds. Table 2 gives bond valence sums at REE^{3+} calculated for six and seven oxygen ligands using parameters reported by Brown and Wu (1976), Zachariasen (1978), and Brown and Altermatt (1985). Using any of these sets of parameters, there is a difference in the sums between sixfold and sevenfold coordination of approximately 0.5 v.u. There is, however, a systematic offset among values predicted using the different parameters, so that no single set accounts for the observed distances. Nevertheless, it is clear that when bond

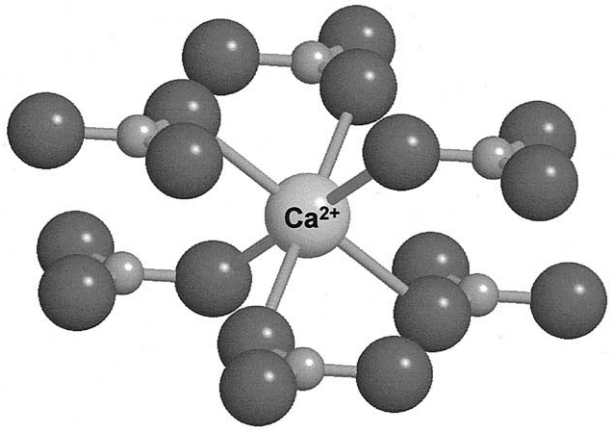

Fig. 5. Schematic model of the calcite structure showing the octahedral coordination of the Ca site.

valence sums for Dy and Yb are in good agreement for sixfold coordination, then Nd and Sm are not in good agreement, and vice versa, when bond valence sums for Nd and Sm are consistent with sevenfold coordination, then those for Dy and Yb are not. For example, using our observed REE-O distances and the bond valence parameters of Zachariasen (1978), trivalent Dy and Yb have sums of 2.99 and 3.07 v.u., respectively, for six oxygen ligands, whereas the bond valence sums at Nd and Sm for six oxygens are only 2.75 and 2.76 v.u., respectively.

The sevenfold coordination of Nd and Sm dopants in calcite requires an additional ligand relative to the octahedral coordination around Ca, which would necessarily disrupt the local structure to some degree. With only one additional ligand, whatever structural disruption exists will be averaged (by EXAFS) with the other oxygens, which are presumably from CO_3 groups having "calcite-like" coordination. This averaging makes it impossible to determine exactly how the additional oxygen ligand is accommodated. However, we can envision a simple means of including an additional oxygen in the first coordination shell from a CO_3 group. In the calcite structure, the six oxygens coordinated to Ca are from six different CO_3 groups, each with a monodentate linkage (Fig. 5). The sevenfold coordination could be achieved if one CO_3 group were to have bidentate coordination without affecting the other CO_3 groups. This could occur with just a rotation or twisting of a CO_3 group. However, it is probable that the aqueous REE carbonate complex, the dominant species in the growth solutions, has the CO_3 in bidentate coordination. Therefore, perhaps it is more likely that the bidentate CO_3 linkage of the aqueous complex is simply retained during incorporation into the structure. This remains speculation, and it should be noted that bidentate linkage would mean that the coordination to an adjacent Ca octahedron would also be altered. Moreover, this means of accommodating the sevenfold coordination does not account for charge compensation.

Another possibility would be the addition of an oxygen, either as OH or H_2O, perhaps retained from the hydration shell. The OH would provide charge compensation if the CO_3 ligands were otherwise unchanged. Our EXAFS results show no indication of increased disorder beyond the first ligand shell for the HREEs vs. the LREEs or vice versa and, therefore, offer little insight to likely mechanisms of charge compensation for the heterovalent substitution of trivalent REE for divalent Ca. Zhong and Mucci (1995) presented strong evidence that cosubstitution of Na^+ (for Ca^{2+}) provided charge balance in their experimental calcites. In our experiments, NH_4^+ (or Na^+ in the

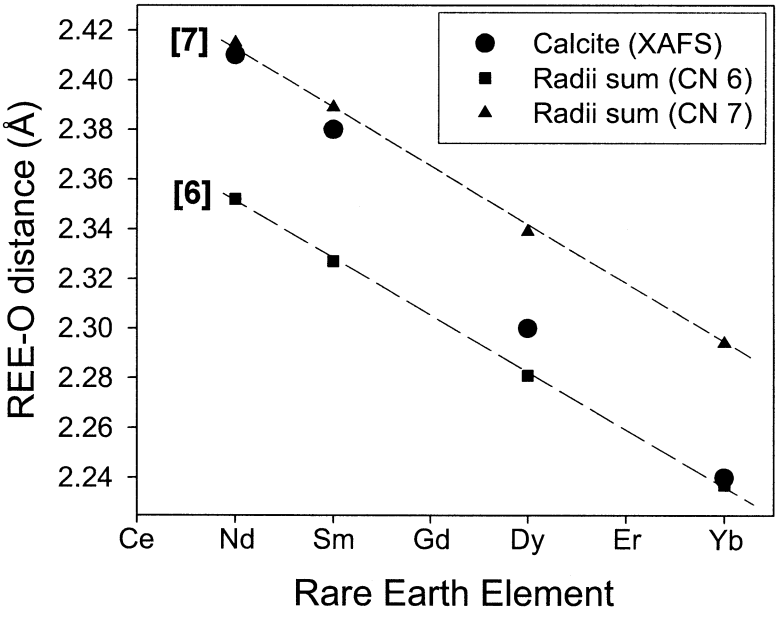

Fig. 6. First-shell REE-O distances in the REE-doped calcites compared with predicted REE-O distances for sixfold and for sevenfold coordination. Predictions based on sum of ionic radii (from Shannon, 1976) and ionic radius for oxygen consistent with coordination as in the calcite structure.

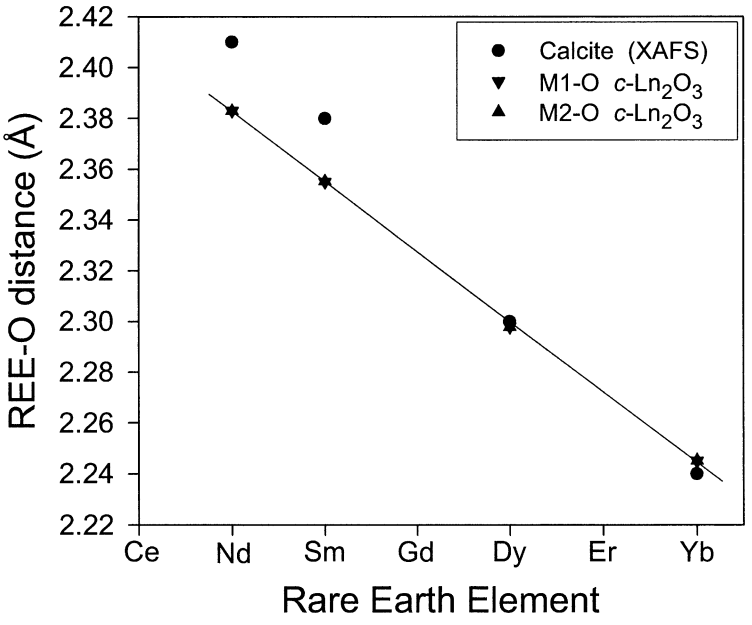

Fig. 7. First-shell REE-O distances in the REE-doped calcites compared with average REE-O distance in the corresponding lanthanide *c*-sesquioxide. Both REE sites in the *c*-sesquioxide have sixfold coordination.

Yb-doped experiments) could have played a similar role. Replacement of one of the six Ca atoms in the shell at ~4.0 Å by N or Na would not be easily discernible from the EXAFS data. There should be increased disorder in the distances for this shell but that might also be expected from the additional oxygen ligand in the Nd- and Sm-doped samples.

In other systems, structural trends across the lanthanide series are commonly found to exhibit differences in REE-O coordination that parallel our present findings for REEs incorporated in calcite. One of the best-studied cases is the coordination number for the lanthanide aquo ions, i.e., the number of H_2O molecules in the first hydration sphere. Although different experimental techniques have resulted in a range of coordination numbers for individual ions, there is a consensus that the LREE aquo ions are ninefold coordinated, whereas the HREE aquo ions are eightfold coordinated (Ohtaki and Radnai, 1993). Aquo ions in the middle of the series appear to have a mixture of eightfold and ninefold coordination, an observation supported by molecular dynamics simulations (Kowall et al., 1995). A preference for a larger coordination number for the LREEs is also observed in the potassium lanthanide carbonates $KREE(CO_3)_2$. Kutlu et al., (1997) determined structures for the Nd, Gd, Dy, Ho, and Yb compounds, showing that two Nd sites occur in $KNd(CO_3)_2$, both having ninefold coordination with a mixture of monodentate and bidentate CO_3 linkage. In the Gd, Dy, Ho, and Yb compounds, a single eightfold-coordinated REE site occurs with exclusively monodentate CO_3 linkage. Beall et al., (1977) documented more subtle coordination differences with REE size in the lanthanide trihydroxide isostructural series $REE(OH)_3$. The metal site is ninefold coordinated (a tricapped trigonal prism) with two distinct REE-O bond distances, apical and equatorial. For the LREEs, the distance to the equatorial oxygens is shorter than to the apical oxygens; for the HREEs, the opposite is true, and the crossover in the series occurs at Gd. Differences in coordination preferences are also evident in the lanthanide sesquioxides for which three forms are known. The *a* modification has sevenfold coordination of the REE, whereas both sites in the *c* modification have sixfold coordination. LREEs La through Sm preferentially adopt the *a* modification, whereas heavier members prefer the *c* modification (Cotton, 1991). The little-studied *b* form is favored at higher temperature. Although none of the examples above may be directly applicable to the REE dopants in calcite, each shows a consistent preference for greater (or different) coordination

Table 2. Bond valence sums for sixfold and sevenfold oxygen coordination of REE^{3+} in calcite.

		Bond Valence Sum at REE^{3+} (v.u.)					
REE	*R* (Å)	BW [6]	BW [7]	ZA [6]	ZA [7]	BA [6]	BA [7]
Nd	2.41	2.75	3.20	2.75	3.21	2.63	3.07
Sm	2.38	2.72	3.17	2.76	3.22	—	—
Dy	2.30	2.87	3.34	2.99	3.49	2.67	3.12
Yb	2.24	2.99	3.48	3.07	3.59	2.85	3.33

Bond valence parameters: BW = Brown and Wu (1976); ZA = Zachariasen (1978); BA = Brown and Altermatt (1985).

for the LREEs, owing to their larger size, relative to the HREEs.

Due to the sevenfold O coordination of Sm and Nd incorporated in the calcite structure, there should be energetic consequences associated with the localized disruption resulting from the presence of the additional O ligand. This should be greater than the energetics associated with a perfectly isomorphous substitution in which the coordination remains unchanged. We presume that this would be a destabilizing effect, so that the overall solubility of a sevenfold-coordinated REE-doped calcite should be greater than if the REE was sixfold coordinated. Hence, it seems probable that Nd and Sm coprecipitated with calcite are more likely to be remobilized (via dissolution) than Dy and Yb. Further speculation about the likely effects on stability must await additional studies. Because the ionic radii of Am^{3+}, Cm^{3+}, and Pu^{3+} are closer to Nd^{3+} and Sm^{3+} than to Dy^{3+} and Yb^{3+}, it is possible that a similar defect structure (and increased solubility) is associated with their incorporation into calcite.

5. CONCLUSIONS

EXAFS data of trivalent Yb, Dy, Sm, and Nd coprecipitated with calcite during crystal growth indicate that these REEs were incorporated in the calcite structure, occupying the Ca site. Comparison of the EXAFS-determined first-shell REE-O distances with the ionic radii from Shannon (1976) indicates a difference in the first-shell REE-O coordination between the LREEs (Nd and Sm) and the HREEs (Dy and Yb). The HREE-O distances are consistent with sixfold O coordination, whereas the LREE-O distances are consistent with sevenfold O coordination. The difference in coordination number of the LREEs incorporated in the calcite structure as compared to the HREEs parallels changes in REE-O coordination along the lanthanide series for other compounds, including aqueous REE species, the potassium lanthanide carbonates, the lanthanide trihydroxide isostructural series, and the lanthanide sesquioxides. The difference between the HREE and LREE oxygen coordinations in calcite possibly reflects differences in the mechanism of charge compensation when substituting trivalent REEs for divalent Ca in the calcite structure and may affect the relative stability of the HREE-calcite solid solutions vs. the LREE-calcite solid solutions.

Acknowledgments—Funding for this work was provided by DOE grant DE-FG07-99ER15013 through the Environmental Management Science Program and by NSF grant EAR9706012. We thank M. Nugent and Y. Lee for assistance with synthesis experiments and K. Pandya (X11A, NSLS) and S. Heald (20-ID-B, APS) for assistance with data collection. Comments from G. Waychunas and two anonymous reviewers improved the final manuscript.

Associate editor: D. L. Sparks

REFERENCES

Beall G. W., Milligan W. O., and Wolcott H. A. (1977) Structural trends in the lanthanide trihydroxides. *J. Inorg. Nucl. Chem.* **39,** 65–70.

Brown I. D. and Wu K. K. (1976) Empirical parameters for calculating cation-oxygen bond valences. *Acta Crystallogr.* **B32,** 1957–1959.

Brown I. D. and Altermatt D. (1985) Bond-valence parameters obtained from a systematic analysis of the inorganic crystal structure database. *Acta Crystallogr.* **B41,** 244–247.

Carroll S. A. (1993) Precipitation of Nd-Ca carbonate solid solution at 25°C. *Geochim. Cosmochim. Acta* **57,** 3383–3393.

Carroll S. A., Bruno J., Petit J-C., and Dran J-C. (1992) Interaction of U(VI), Nd, and Th(IV) at the calcite-solution interface. *Radiochim. Acta* **58/59,** 245–252.

Cheng L., Sturchio N. C., and Bedzyk M. J. (2001) Impurity structure in a molecular ionic crystal: Atomic-scale x-ray study of $CaCO_3$: Mn^{2+}. *Phys. Rev. B* **63,** 144104-1–144104-6.

Cotton S. (1991) *Lanthanides and Actinides*. Oxford Univ. Press, New York.

D'Angelo P., Pavel N. V., and Borowski M. (2001) K- and L-edge XAFS determination of the local structure of aqueous Nd(III) and Eu(III). *J. Synchrotron Radiat.* **8,** 666–668.

Davis J. A., Fuller C. C., and Cook A. D. (1987) A model for trace metal sorption processes at the calcite surface: Adsorption of Cd^{2+} and subsequent solid solution formation. *Geochim. Cosmochim. Acta* **51,** 1477–1490.

Galoisy L. (1996) Local versus average structure around cations in minerals from spectroscopic and diffraction measurements. *Phys. Chem. Miner.* **23,** 217–225.

Gruzensky P. M. (1967) Growth of calcite crystals. In *Crystal Growth* (ed. H. S. Peiser), pp. 365–367, Pergamon Press, New York.

Hanic F., Hartmanova M., Knab G. G., Ursovskaya A. A., and Bagdasarov K. S. (1984) Real structure of Y_2O_3 single crystals. *Acta Crystallogr.* **B40,** 76–82.

Kutlu I., Kalz H. J., Wartchow R., Ehrhardt H., Seidel H., and Meyer G. (1997) Kalium-lanthanoid-carbonate, $KM(CO_3)_2$ (M = Nd, Gd, Dy, Ho, Yb). *Z. Anorg. Allg. Chem.* **623,** 1753–1758.

Lee J. H. and Byrne R. H. (1993) Complexation of trivalent-rare-earth elements (Ce, Eu, Dg, Tb, Yb) by carbonate ions. *Geochim. Cosmochim. Acta* **57,** 295–302.

Lee Y. J., Reeder R. J., Wenskus R. W., Elzinga E. J. (2002). Structural relaxation in the $MnCO_3$-$CaCO_3$ solid solution: A Mn K-edge EXAFS study. *Physics Chem. Miner.* (in review).

Maslen E. N., Streltsov V. A., and Ishizawa N. (1996) A synchrotron X-ray study of the electron density in c-type rare earth oxides. *Acta Crystallogr.* **B52,** 414–422.

Mason R. A. and Mariano A. N. (1990) Cathodoluminescence activation in manganese-bearing and rare earth-bearing synthetic calcites. *Chem. Geol.* **88,** 191–206.

Millero F. J. (1992) Stability-constants for the formation of rare-earth inorganic complexes as a function of ionic-strength. *Geochim. Cosmochim. Acta.* **56,** 3123–3132.

Palmer M. R. (1985) Rare earth elements in foraminifera tests. *Earth Planet. Sci. Lett.* **73,** 285–298.

Paquette J. and Reeder R. J. (1995) Relationship between surface structure, growth mechanism, and trace element incorporation in calcite. *Geochim. Cosmochim. Acta* **59,** 735–749.

Parekh P. P., Möller P., Dukski P., and Bausch W. M. (1977) Distribution of trace elements between carbonate and non-carbonate phases of limestone. *Earth Planet. Sci. Lett.* **34,** 39–50.

Reeder R. J. (1996) Interaction of divalent cobalt, zinc, cadmium, and barium with the calcite surface during layer growth. *Geochim. Cosmochim. Acta* **60,** 1543–1552.

Reeder R. J., Lamble G. M., and Northrup P. A. (1999) XAFS study of the coordination and local relaxation around Co^{2+}, Zn^{2+}, Pb^{2+}, and Ba^{2+} trace elements. *Am. Mineral.* **84,** 1049–1060.

Reeder R. J., Nugent M., Tait C. D., Morris D. E., Heald S. M., Beck K. M., Hess W. P., and Lanzirotti A. (2001) Coprecipitation of uranium (VI) with calcite; XAFS, micro-XAS, and Luminescence characterization. *Geochim. Cosmochim. Acta* **65,** 3491–3503.

Ressler T. (1997) WinXAS: A new software package not only for the analysis of energy-dispersive XAS data. *J. Phys. IV* **7,** C2–269.

Schleid T. and Meyer G. (1989) Single-crystals of rare-earth oxides from reducing halide melts. *J. Less-Common Met.* **149,** 73–80.

Shannon R. D. (1976) Revised effective ionic radii and systematic studies of interatomic distances in halides and chalcogenides. *Acta Crystallogr.* **A32,** 751–767.

Solera J. A., Garcia J., and Proietti M. G. (1995) Multielectron excitations at the *L* edges in rare earth ionic aqueous solutions. *Phys. Rev.* **B51,** 2678–2686.

Terakado Y. and Masuda A. (1988) The coprecipitation of rare-earth elements with calcite and aragonite. *Chem. Geol.* **69,** 103–110.

Wood S. A. (1990) The aqueous geochemistry of the rare-earth elements and yttrium. 1. Review of available low-temperature data for inorganic complexes and the inorganic REE speciation of natural waters. *Chem. Geol*. **82,** 159–186.

Xu N., Hochella M. F., Brown G. E., Parks G. A. (1996) Co(II) sorption at the calcite-water interface: I. X-ray photoelectron spectroscopic study. *Geochim. Cosmochim. Acta.* 2801–2815.

Zabinsky S. I., Rehr J. J., Ankudinov A., Albers R. C., and Eller M. J. (1995) Multiple-scattering calculations of X-ray absorption spectra. *Phys. Rev.* **B52,** 2995–3009.

Zachariasen W. H. (1978) Bond lengths in oxygen and halogen compounds of d and f elements. *J. Less-Common Met.* **62,** 1–7.

Zhong S. and Mucci A. (1995) Partitioning of rare earth elements (REEs) between calcite and seawater solutions at 25°C. *Geochim. Cosmochim. Acta* **59,** 443–453.